# Response of an Overhead Wire Near a NEMP Simulator

DIETHARD HANSEN, MEMBER, IEEE, HANS SCHAER, DIETRICH KOENIGSTEIN, HENK HOITINK, HEYNO GARBE, AND D. V. GIRI, SENIOR MEMBER, IEEE

*Abstract*—**The response of an overhead wire illuminated by a simulated nuclear electromagnetic pulse (NEMP) has been experimentally investigated. The wire is 70-m long, 7 mm in diameter, and is situated 5 m above the ground. It is located 20 m away from a hybrid type of EMP simulator. The simulator is a resistively loaded elliptical loop structure with its pulse generator located 20 m above the ground. The overhead wire is terminated with various combinations of short circuit, open circuit, and characteristic impedance at the two ends, and the current response is measured at one end and in the middle. The measured responses are compared with calculated values from available analytical models.**

## I. Introduction

OVERHEAD wires and cables carry electric power, communication signals etc., to and from civilian and military facilities located both above the ground and underground. They are integral components of a vast array of facilities that may be exposed to hostile electromagnetic (EM) environments both manmade and natural. A clear understanding of their interaction with the EM environment is essential for designers concerned with a system's ability to survive the environment. The overhead wire's response to incident EM radiation has been theoretically known [1]–[3], and in the present work, we have focused on measuring such responses. The analytical models, for example [1] and [3], have a similar approach in arriving at the response. They treat the bare wire or shielded wire above ground (with soil as a return conductor) as a "two-wire" transmission line. The characteristic impedance $Z_c$ and the propagation number $\gamma$ of this equivalent two-wire line is known [4] in terms of the geometrical parameters and the constitutive parameters of the soil and the cable shield, if any. Then, the distributed voltage source in the Telegrapher's equations [5] is obtained from the longitudinal component (which is parallel to the overhead wire) of the electric field. This driving electric field is a sum of incident and ground-reflected fields in the absence of the wire or the cable.

The measurements reported in this paper were performed on an overhead wire near the "mobile" electromagnetic pulse simulator (MEMPS) in Spiez, Switzerland. MEMPS is operated and maintained by the AC Laboratory of the Swiss Department of Defense. MEMPS is an elliptical loop hybrid type of EMP simulator that is about 20-m high and 60-m wide. The loop structure is resistively loaded and can be excited by a 4-MV pulser, which is capable of producing an approximately 80-kV/m electric field, with a 7-ns rise time directly below the pulser [6]. The overhead wire is, however, located at a horizontal distance 20 m away from the simulator and 5 m above the ground where the horizontal $E$ field is of the order of 25 kV/m. The transmission line formed by the wire with soil as the return conductor is terminated in various combinations of short circuit, open circuit, and the characteristic impedance during the experiment. All three components of the incident electric field are computed, and they are also measured at a few locations near the transmission line. Coupling these fields to the transmission line, produced transmission line currents are computed using the transmission line theory of [1] and measured as well. Comparisons of the calculated and measured responses are made.

An additional feature during the experiment was the presence of a 15-m long, 3-m wide, 4.5-m high locomotive of the Swiss Federal Railway Company (SBB) at the center of the 70-m long transmission line. The locomotive was 4.5-m high compared with the 5-m height of the overhead wire, and there was no electrical connection between the wire and the locomotive. The presence of the locomotive impacts the wave impedance of the transmission line and at least locally disturbs the fields coupling to the line. This was empirically accounted for in the coupling computations, which resulted in better agreement between theory and experiment. The various sections of this paper describe the incident field computation and measurement (Section II), the experimental configurations and measurement schemes (Section III), the analytical model (Section IV), and comparisons between the theoretical predictions and measurements (Section V).

## II. The Incident Field from MEMPS

A generic hybrid type of EMP simulator is shown in Fig. 1. The dimensions of 20-m height and 60-m width shown are for the Swiss MEMPS. The structure is energized by an EMP pulser at the top, as indicated in Fig. 1. At low frequencies, where the wavelengths are large compared with simulator structure, a quasi-static form of the fields is applicable. The high-frequency (early-time) portion of the waveform reaching the system under test is radiated from a relatively small-source region, which is typically a biconical radiator in the pulser it-

Manuscript received October, 22, 1988; revised June 26, 1989. This work was supported by the Swiss Armament Technology and Procurement Group, Spiez (Swiss Department of Defense), and the Swiss Federal Railway Company.

D. Hansen, H. Schear, D. Koenigstein, H. Hoitink, and H. Garbe are with Asea Brown Boveri Ltd., ABB EMI Control Center, Baden, Switzerland.

D. V. Giri is with Pro-Tech, Berkeley, CA 94710.

IEEE Log Number 8931967.

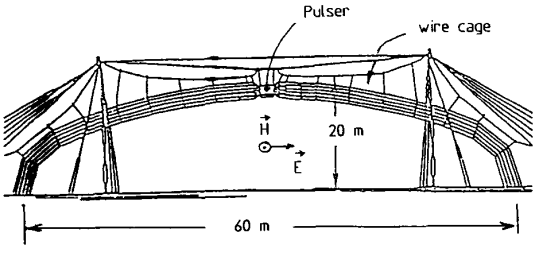


Fig. 1. Generic hybrid-type of EMP simulator showing the dimensions for MEMPS (not to scale).

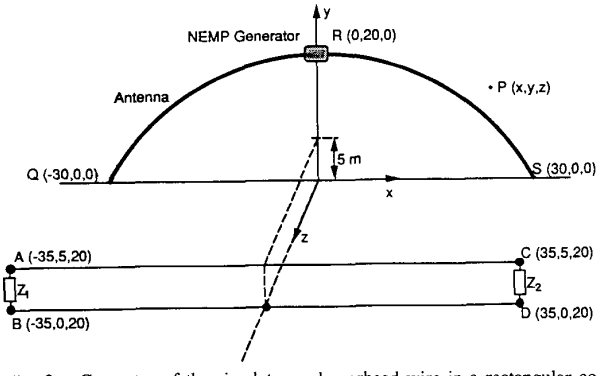


Fig. 2. Geometry of the simulator and overhead wire in a rectangular coordinate system (the coordinates of various points are in meters).

self. The low-frequency (late time) portion of the waveform is associated with the currents and charges distributed over the major dimensions of the simulator structure. The structure is made sparse to avoid high-frequency reflections off the structure, and it is also impedance loaded to dampen the structure resonances in the intermediate frequency regime.

A rectangular coordinate system $(x, y, z)$, with its origin on the ground directly underneath the pulser is defined, as is shown in Fig. 2. The location of the overhead wire is also indicated. This wire is located at a height of 5 m above the ground and 20 m away from the simulator structure in the $z$ direction. For the purpose of evaluating the wire response, one requires the incident field at the location of the wire in its absence. Such an incident field is available to us from two sources: computed and measured. The computations are based on a method-of-moments approach [7] for an arbitrary distribution of loaded or unloaded thin-wire structures. The computations were made for all three components $E_x$, $E_y$, $E_z$ at three locations $P_1$ (0, 4.5, 20 m), $P_2$ (−17.5, 4.5, 20 m), and $P_3$ (−35, 4.5, 20 m).

Recall that $z = 20$ m is the vertical plane containing the axis of the overhead wire. The three points are located on a horizontal line 0.5-m below and parallel to the wire at one end of the wire, at the center, and at a point in between. The computations are of course symmetric in the right half of the overhead wire region.

A limitation of this computational approach is the use of perfectly conducting ($\sigma_g = \infty$) ground. The electric field distribution along the transmission line was computed under the following assumptions:

1) double exponential pulser voltage

$$V_p(t) \approx V_0[e^{-\alpha t} - e^{-\beta t}]u(t) \tag{1}$$

with

$V_0$ arbitrary
$\alpha =$ $4 \times 10^6$/s
$\beta =$ $4.8 \times 10^8$/s
$u(t) \equiv$ unit step function

2) $\sigma_g \equiv$ conductivity of ground $= \infty$
3) resistive loading of the elliptical structure.

It is noted that $\sigma_g = \infty$ is used for the present incident field computation only. Once the incident field model is established, the actual overhead wire response computations account for finite soil conductivity.

The computed electric field quantities are shown in Fig. 3. Recall that the axis of the overhead wire is located in the $z = 20$ m plane. Fig. 3 also indicates the locations of the test points $P_1$, $P_2$, and $P_3$ relative to the wire above the ground in this plane. The top three plots in Fig. 3 are the axial (parallel to the wire) components of the electric field, and the bottom three plots are components of the electric field parallel to the terminators. It is observed that the principal horizontal component $E_x(x, y, z)$ is fairly uniform along the overhead wire, and the vertical component has relatively more variation along the wire.

Since the axial electric field is the dominant driver, which results in distributed voltage sources along the wire, we have focused our attention on this component of the incident field. From an earlier field mapping effort in and near the simulator facility, the axial electric field $E_x$ was available at a few locations near the wire location. These measured axial electric fields are shown plotted in Fig. 4. Fig. 4 illustrates the fairly uniform excitation of the overhead wire.

However, an additional feature in our experiment was the presence of an electrical locomotive of the SBB at the center of the transmission line. The locomotive's dimensions are length = 15.4 m, height = 3.8 m, and width = 2.9 m. Electromagnetically, the locomotive's presence complicates the situation by impedance loading the transmission line and, more importantly, by distorting the incident field illuminating the line.

Since the length of the overhead wire is about 4.5 times larger than the length of the locomotive, it is possible to account for its presence by localized corrections to the excitation fields. In other words, the 70-m length of the transmission line may be divided into three sections, with the middle 15-m-long section extending over the length of the locomotive and two sections on either side, which are 27.5 m long. A localized correction may be applied to the middle section only to account for the presence of the locomotive. Such a correction to the incident field has resulted in better comparisons between the computations and experimental responses, as is seen later in this paper.

Returning to the subject of an empirical model for the mea-

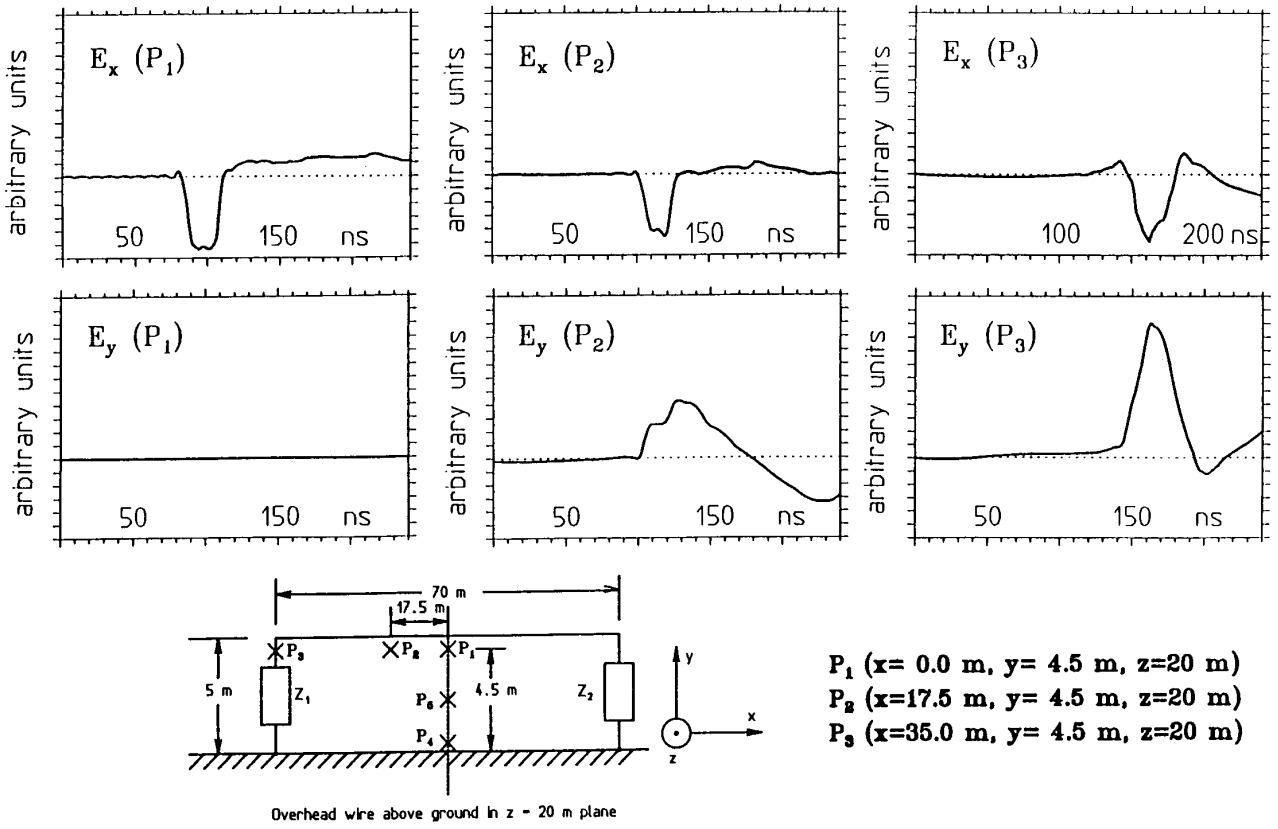


Fig. 3. Computed components (parallel to wire in $x$ direction and parallel to the terminator in $y$ direction) of the electric field. Note: The units of $E_x$ and $E_y$ at $P_1$, $P_2$, and $P_3$ are the same.

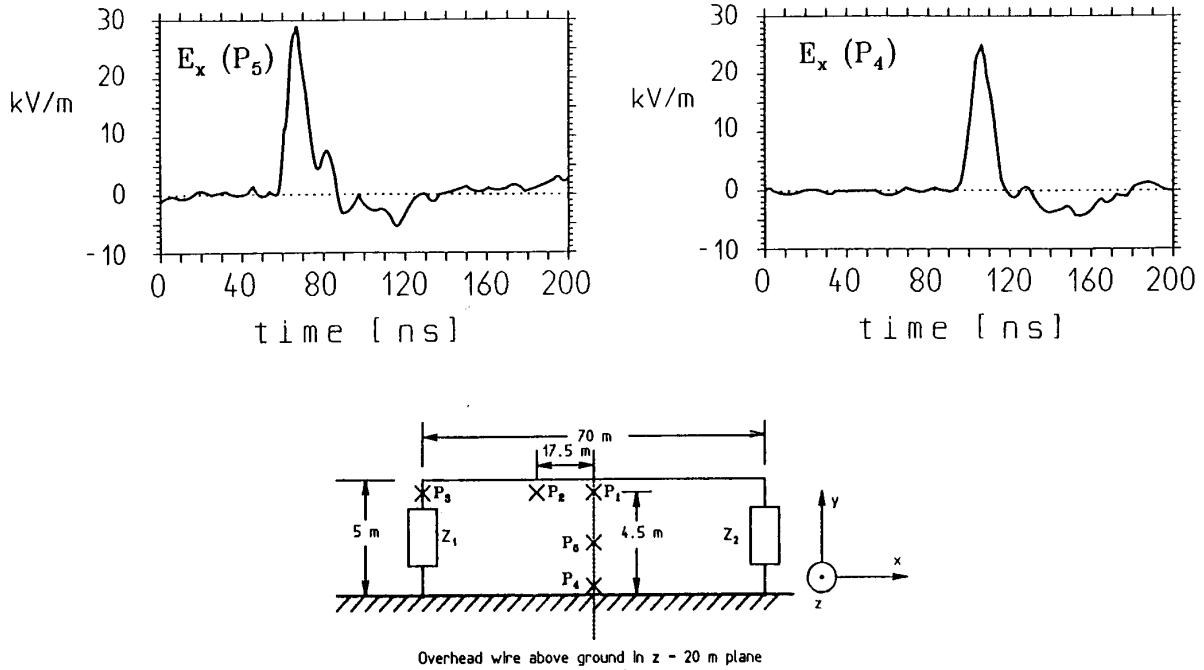


Fig. 4. Measured component of the incident electric fields at test points $P_4$ and $P_5$ (available from previous field mapping data at MEMPS): $P_4$ ($x = 0$, $y = 0.5$ m, $z = 22.5$ m); and $P_5$ ($x = 0$, $y = 2.4$ m, $z = 22.5$ m).

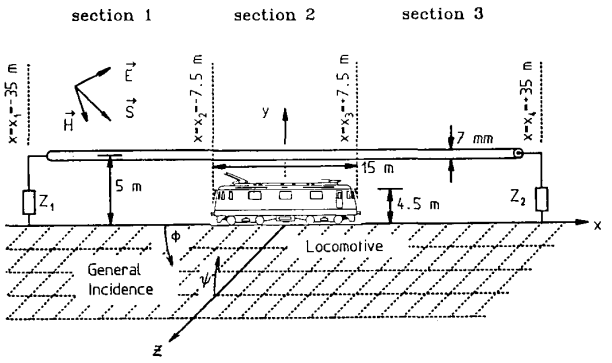


Fig. 5. Overhead wire over soil in the $z = 20$-m plane showing the three sections over which the axial $E_x$ field is considered uniform. Note: The width of the locomotive along the $z$ direction is 3 m, but this information is unused.

sured $E_x$ field, it is observed that this field is fairly uniform over the entire length of the wire in the absence of the wire and the locomotive. Consequently, a double exponential model is proposed and used for the purpose of coupling calculations. Therefore, the uniform excitation field can now be approximately modeled by

$$E_x(t) \approx E_o(e^{-\alpha t} - e^{-\beta t})u(t) \tag{2}$$

with $E_o = 25$ kV/m, $\alpha = 4 \times 10^6$/s, and $\beta = 4.8 \times 10^8$/s. As described above, this field is incident on the two end sections, and a corrected field of the same form is incident in the middle section. The illuminating fields in various sections of the wire illustrated in Fig. 5 are empirically given by

$$E_x(x, 4.5m, 20m, t) \approx f(x)E_o(e^{-\alpha t} - e^{-\beta t})u(t). \tag{3}$$

It is observed that the $x$ dependence is approximated by

$$f(x) = \begin{cases} 1 & x_1 \le x \le x_2 \\ f_2 & x_2 < x < x_3 \\ 1 & x_3 \le x \le x_4 \end{cases}$$

where $x_1$, $x_2$, $x_3$, and $x_4$ are shown in Fig. 5. Recall that $E_o$, $\alpha$, and $\beta$ are postulated earlier, and $u(t)$ is a unit step function of time. The impact of approximating the incident field by the above model is discussed in further detail in Section V. Specifically, we have studied the effect of changing $\alpha$ and $\beta$ on the eventual current responses. It is, however, emphasized that the above model is for the primary incident field in the absence of the wire, and the total horizontal field is constructed by adding the ground reflections.

## III. The Overhead Wire and Experimental Configurations

Fig. 2 has shown the geometry of the simulator and the overhead wire in a rectangular coordinate system, and Fig. 5 shows the location and relevant dimensions of the locomotive present during the experiment. Since the wire and the simulator are fixed in their positions, the angle of incidence and polarization of the incident field are fixed. The parameters that can and have been varied in the experiment are:

TABLE I
Experimental Parameters

| Case # | Location x(m) along the wire where the current is measured | Terminating Impedances $Z_1$ ($\Omega$) ($L = 5$ $\mu$H) | $Z_2$ ($\Omega$) |
|---|---|---|---|
| 1 | x = -35 m | 600 + jωL | 600 + jωL |
| 2 | x = -7 m | 600 + jωL | 600 + jωL |
| 3 | x = -35 m | 600 + jωL | $10^6$ |
| 4 | x = -7 m | 600 + jωL | $10^6$ |
| 5 | x = -7 m | $10^6$ | 600 + jωL |
| 6 | x = -35 m | 600 + jωL | .002 + jωL |
| 7 | x = -7 m | 600 + jωL | .002 + jωL |
| 8 | x = -7 m | $10^6$ | $10^6$ |
| 9 | x = -35 m | .002 + jωL | .002 + jωL |
| 10 | x = -7 m | .002 + jωL | .002 + jωL |

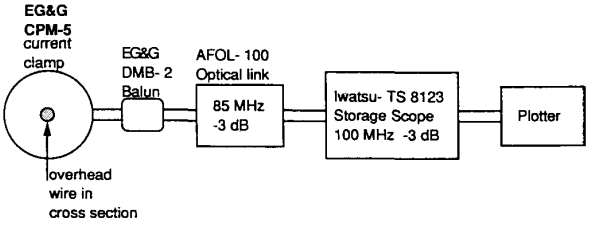


Fig. 6. Block diagram of the experimental setup for current measurement.

a) the location along the wire where the current response is measured and b) the terminating impedances $Z_1$ and $Z_2$ on the two ends of the overhead wire. Ten different experimental configurations have been studied, and the experimental parameters have been listed in Table I. The various choices in the experimental parameters are described below.

First of all, the two locations where the induced currents are measured are $x = -35$ m and $x = -7$ m, corresponding respectively to the end of the line and just above the left edge of the locomotive. The block diagram of the current measurement experiment is shown in Fig. 6. Second, the terminating impedances $Z_1$ and $Z_2$ are governed by a requirement for a short circuit, open circuit, and the wave impedances. Several combinations are possible, and some choices have been made. It is noted, however, that the leads connecting the terminators have a combined inductance of $\sim 5$ $\mu$H, which is estimated on the basis of 1 $\mu$H/m and a resistance of 2 m$\Omega$. Consequently, a nominal short circuit becomes $0.002\ \Omega + j\ (5\ \mu\text{H})$.

## IV. Analytical Model Used for Comparison

For an aerial wire of radius $a$ and height $h$ above the ground, the expressions for the characteristic impedance $\tilde{Z}_c$ and the propagation constant $\gamma$ are available in [1] and [4], with and without neglecting the series impedance $\tilde{Z}_g$ and shunt admittance $\tilde{Y}_g$ of the ground medium. After computing $\tilde{Z}_c$ (with and without $\tilde{Z}_g$ and $\tilde{Y}_g$) and observing its low-frequency behavior, we determined that 600 $\Omega$ is a reasonable value for terminating the overhead wire to "ground." The terminating impedances at both ends $\tilde{Z}_1$ and $\tilde{Z}_2$ are varied (short circuit, open circuit, and 600 $\Omega$).

With regard to the analytical model for estimating the over-

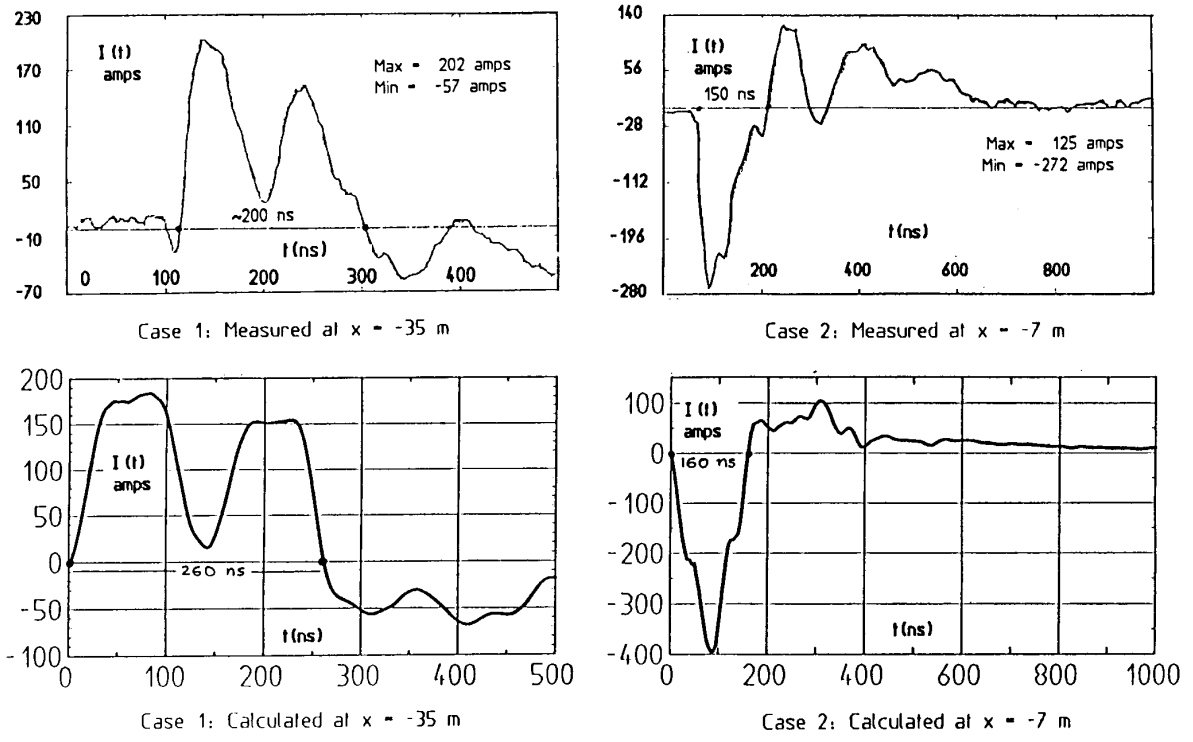


Fig. 7. Calculated and measured current responses (cases 1 and 2): $Z_1 = Z_2 = 600 + j\omega L$ with $L = 5\ \mu$H.

head wire response, it is simply observed that the current along the wire, for harmonically varying signals ($\exp(j\omega t)$), satisfies the following second-order differential equation

$$\frac{d^2\tilde{I}}{dx^2} - \gamma^2\tilde{I} = -\tilde{Y}'\tilde{E}_x(x, \omega) \tag{4}$$

where $\gamma^2 = \tilde{Z}'\tilde{Y}'$ with $\tilde{Z}'$ and $\tilde{Y}'$ being the per-unit-length impedances and admittances. The forcing function $\tilde{E}_x(x, \omega)$ is a sum of incident plus ground-reflected fields. The response $\tilde{I}$, which is the solution of the above differential equation, may be written as

$$\tilde{I}(x, \omega) = [\tilde{K}_1 + \tilde{P}(x)]e^{-\gamma x} + [\tilde{K}_2 + \tilde{Q}(x)]e^{\gamma x} \tag{5}$$

where $\tilde{P}(x)$ and $\tilde{Q}(x)$ are known [1] integral functions of the forcing function $\tilde{E}_x$. $\tilde{K}_1$ and $\tilde{K}_2$ are determined from the terminating impedances $\tilde{Z}_1$ and $\tilde{Z}_2$ at the two ends.

Since the expressions for $\tilde{E}_x$, $\tilde{P}$, $\tilde{Q}$, $\tilde{K}_1$, and $\tilde{K}_2$ are well documented in [1], they are not repeated here. We have simply developed and used computer routines for estimating the wire responses for a given set of ground parameters, incident field, and terminating impedances.

## V. Comparison of Theoretical and Experimental Results

The ten experimental configurations investigated in our study have been identified in Table I as cases 1 to 10. The measurement of current is performed at two locations ($x = -35$ m and $x = -7$ m), while the terminations are varied, as listed in Table I. The results (measured and calculated) are presented in Figs. 7 to 11. The top portion of these figures contains measured data in time domain, and the bottom portion contains the corresponding computed data. Several comments concerning these comparisons are in order.

First of all, it is observed that the comparisons in general are fair, and there is a good qualitative agreement and some deviations quantitatively. The dip after the first peak (e.g., cases 1, 3 etc.) needs explanation, as does the choice of soil conductivity $\sigma_g$.

### A. Choice of Ground Parameters

With regard to the soil or ground conductivity, it affects

a) total electric field above the ground, which accounts for the ground reflection;
b) the characteristic impedance of the transmission line; and
c) the propagation factor.

To arrive at the choice of $\sigma_g$, different values of

$$\sigma_g = \infty,\ 10^{-1},\ 10^{-2},\ 10^{-3}\Omega^{-1}/\text{m}$$

were used in a numerical experiment in computing the total horizontal electric field and the induced current in the transmission line for case 1. These results may be seen in Figs. 12 and 13, which lead us to use $\sigma_g = 0.01\ \Omega^{-1}/\text{m}$. $\epsilon_r$ was also varied, as is seen in Fig. 14. The overhead wire response for case 1 is insensitive to $\epsilon_r$ values in the range of 1 to 10.

It is noted that although $\sigma_g$ is varied, the peak amplitude of the horizontal total electric field is unchanged, but the zero

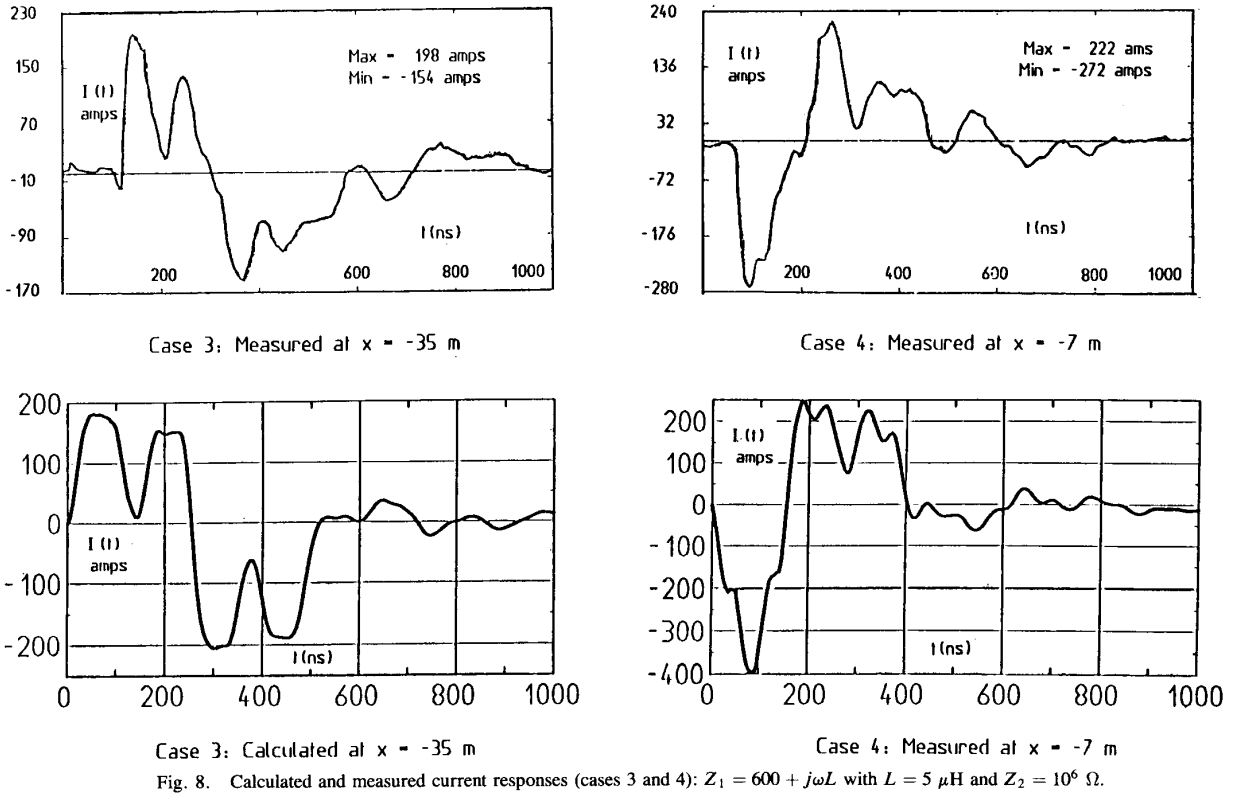


Fig. 8. Calculated and measured current responses (cases 3 and 4): $Z_1 = 600 + j\omega L$ with $L = 5\ \mu$H and $Z_2 = 10^6\ \Omega$.

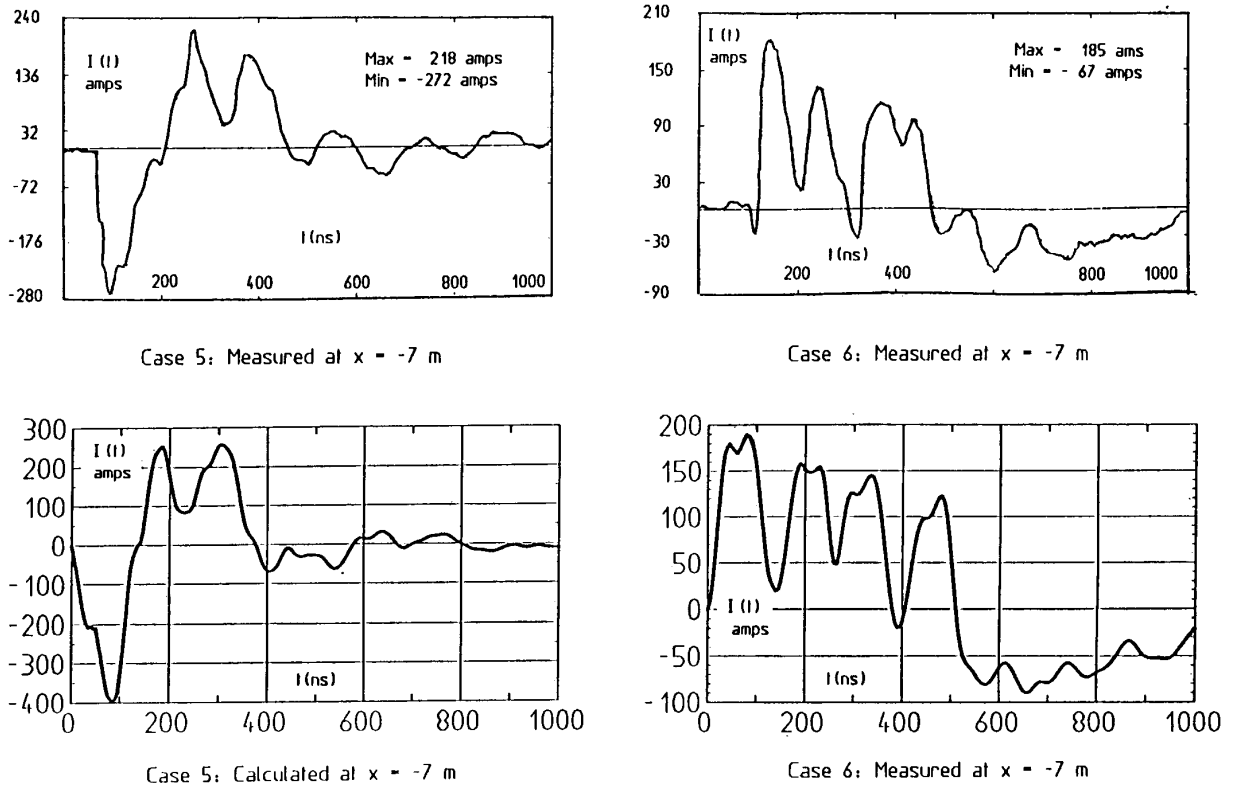


Fig. 9. Calculated and measured current responses (cases 5 and 6): Case 5–$Z_1 = 10^6\ \Omega$ and $Z_2 = 600 + j\omega L$ with $L = 5\ \mu$H; case 6–$Z_1 = 600 + j\omega L$ and $Z_2 = 0.002 + j\omega L$ with $L = 5\ \mu$H.

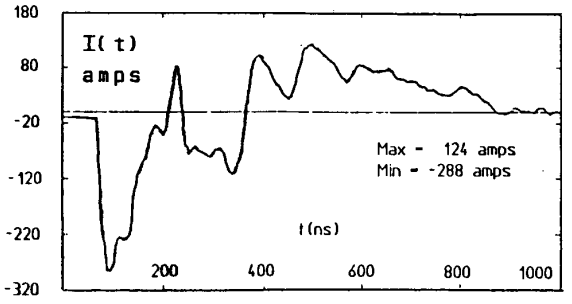


Case 7: Measured at x = -7 m

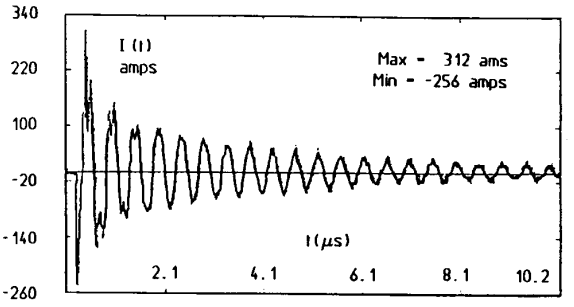


Case 8: Measured at x = -7 m

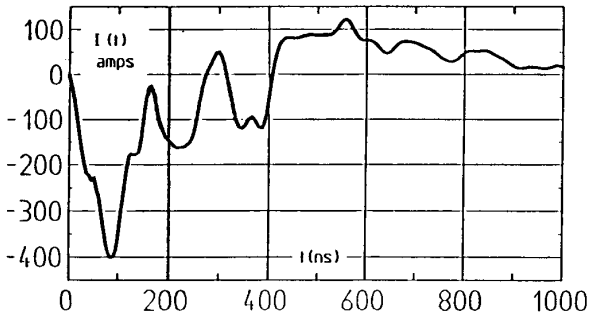


Case 7: Calculated at x = -7 m

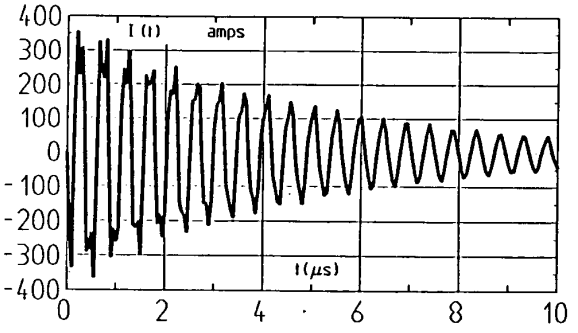


Case 8: Measured at x = -7 m

Fig. 10. Calculated and measured current responses (cases 7 and 8): Case 7-$Z_1 = 600 + j\omega L$ and $Z_2 = 0.002 + j\omega L$ with $L = 5$ $\mu$H; case 8-$Z_1 = Z_2 = 10^6$ $\Omega$.

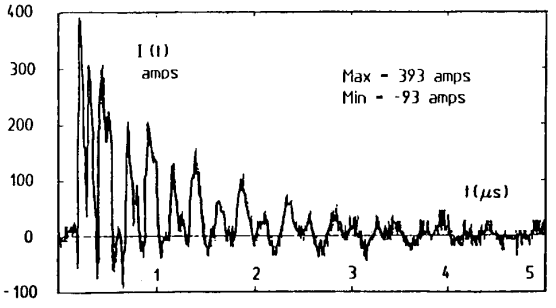


Case 9: Measured at x = -35 m

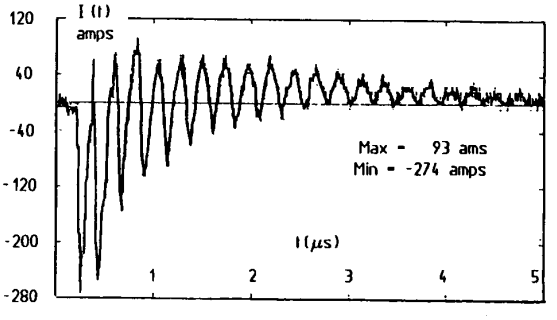


Case 10: Measured at x = -7 m

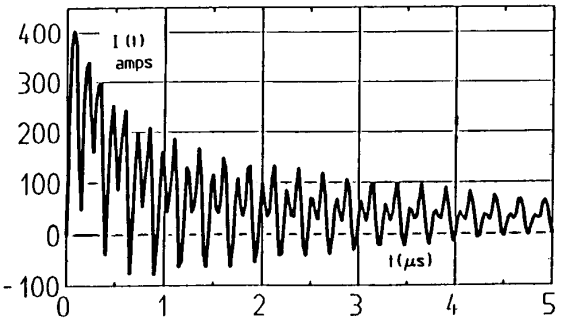


Case 9: Calculated at x = -35 m

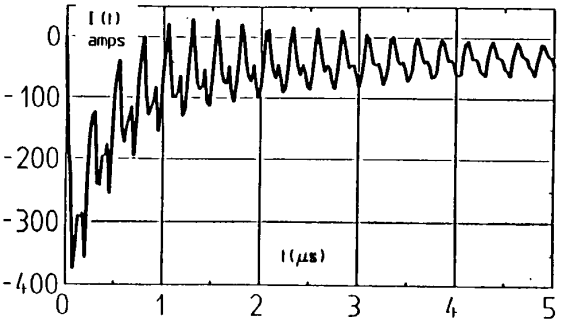


Case 10: Measured at x = -7 m

Fig. 11. Calculated and measured current responses (cases 9 and 10): $Z_1$ and $Z_2 = 0.002 + j\omega L$ with $L = 5$ $\mu$H.

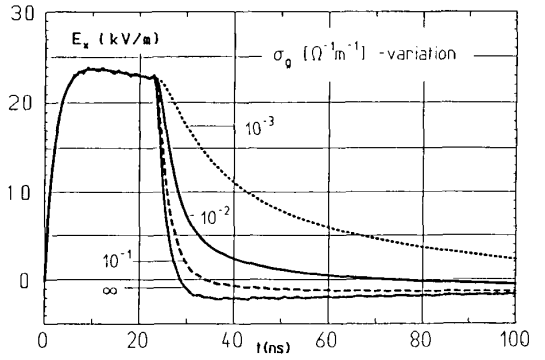


Fig. 12. Horizontal electric field after ground reflection at a height of 5 m above ground with varying $\sigma_g$.

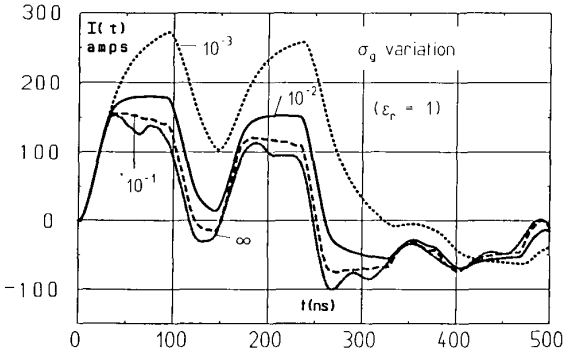


Fig. 13. Induced current (computed) for case 1 with varying $\sigma_g$.

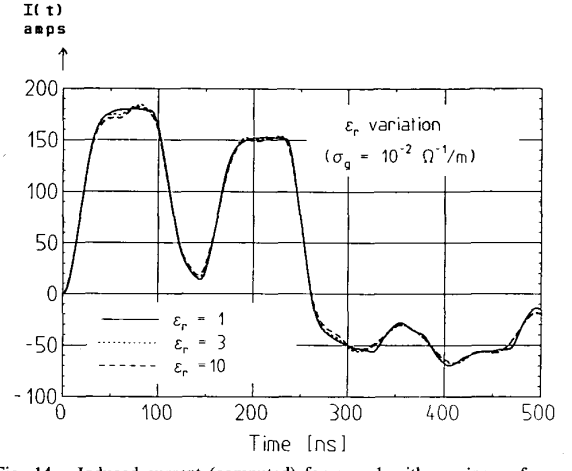


Fig. 14. Induced current (computed) for case 1 with varying $\epsilon_r$ for $\sigma_g = 10^{-2}\ \Omega^{-1}$/m. Note: The induced current is sensitive for $\epsilon_r$ variation between 1 and 10.

crossing is significantly affected. On the other hand, in the induced current, there is approximately a factor-of-2 variation for $\sigma_g$ changing from $\infty$ to $10^{-3}$, and a $\sigma_g$ value of $10^{-2}$ $\Omega^{-1}$/m appears to give the best comparison with experimental results with $\epsilon_r$ of any value between 1 and 10. We have used $\sigma_g = 10^{-2}\ \Omega^{-1}$/m and $\epsilon_r = 1$ for our comparisons, and the theoretical calculations will be insignificantly different if we chose $\sigma_g = 10^{-2}\ \Omega^{-1}$/m and $\epsilon_r = 10$.

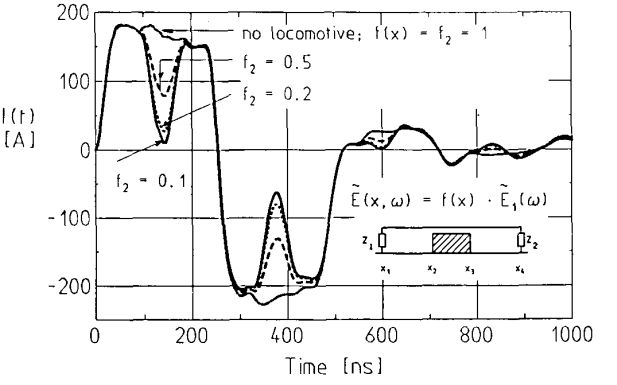


Fig. 15. Induced current $I(t)$ in amps, computed for case 3 (Table I), with varying value of $f_2(3)$.

### B. Local Field Variations

The subject of localized electric field variation due to the presence of the locomotive has been discussed earlier (see Fig. 5) in (3), where a position-dependent constant was introduced. The constant $f_2$ in section 2 of Fig. 5 was varied in a set of numerical experiments shown in Fig. 15. Once again, the conclusion was that $f_2 = 0.1$ leads us to the best comparison with experimental results. It is pointed out that the empirical constant $f_2$ accounts for the presence of the locomotive while computing the response of the overhead wire.

### C. Temporal Behavior of the Incident Field

As was mentioned at the end of Section II, the transmission line current responses have been computed using a double exponential nuclear EMP (NEMP) incident field of the form

$$E_o(e^{-\alpha t} - e^{-\beta t})u(t)$$

with

$$\alpha = 4 \times 10^6/\text{s}$$

$$\beta = 4.8 \times 10^8/\text{s}.$$

However, it is well known that the MEMPS-like facility cannot generate a double-exponential type of field exactly, so the question arises whether a moderate variation in $\alpha$ and $\beta$ can lead to small or large variations in the transmission line currents. $\alpha$ was varied in steps from $2 \times 10^6$/s, $4 \times 10^6$/s, and $8 \times 10^6$/s, keeping $\beta$ fixed at $4.8 \times 10^8$/s. For these three cases, the total horizontal electric field (incident double exponential plus ground reflections) and the induced current in the transmission line are computed. These are shown in the top half of Fig. 16. Next, we studied the impact of changing $\beta$ values from $1 \times 10^8$/s, $4.8 \times 10^8$/s, and $1 \times 10^9$/s, keeping $\alpha$ fixed at $4 \times 10^6$/s. Similar calculations of the total field and induced current were performed, and the results are shown in the bottom part of Fig. 16. The ground characteristics ($\epsilon_r = 1$ and $\sigma_g = 10^{-2}\ \Omega^{-1}$/m) are held fixed during these computations.

From the above numerical experiments, it is observed that the electric field component parallel to the transmission line is not significantly affected by a moderate variation in $\alpha$ and $\beta$

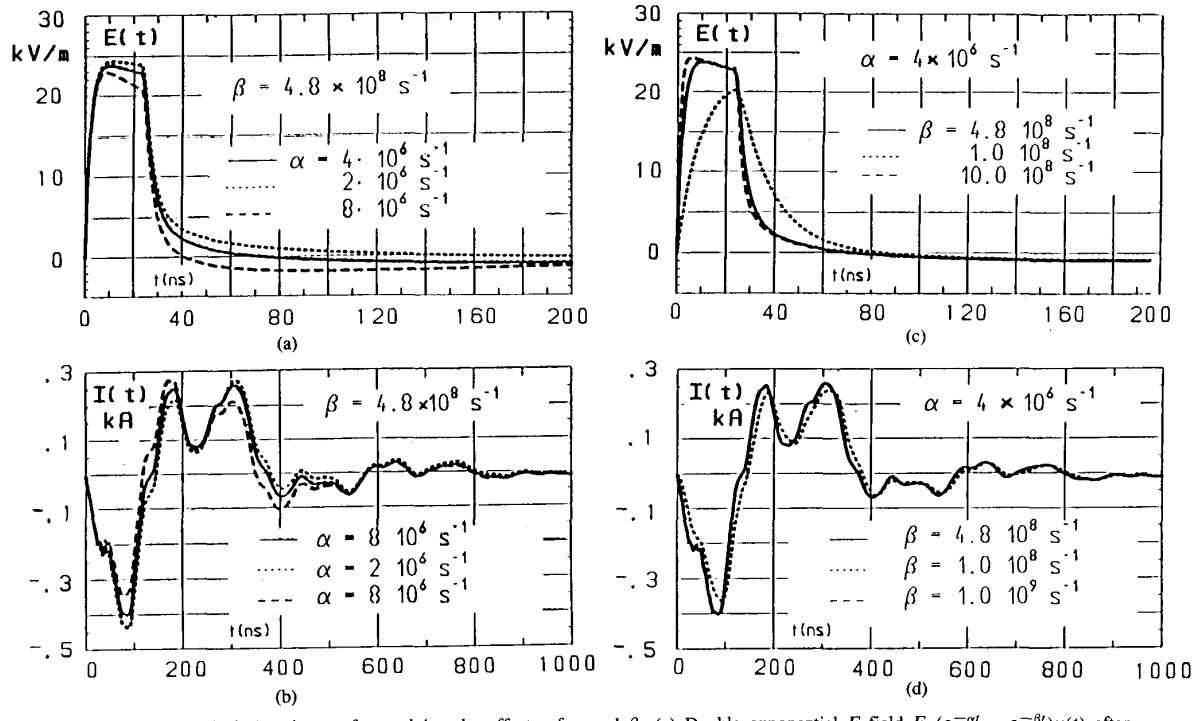


Fig. 16. Numerical experiments for studying the effects of $\alpha$ and $\beta$: (a) Double exponential $E$ field $E_o(e^{-\alpha t} - e^{-\beta t})u(t)$ after reflection at ground ($\sigma_g = 10^{-2}\ \Omega^{-1}$/m, $\epsilon_r = 1 \cdots 10$) for various values of $\alpha$ at $h = 5$ m above ground; (b) induced current in transmission line corresponding to $\alpha$ values in (a) case 5 of Fig. 9 for comparison; (c) double exponential $E$ field $E_o(e^{-\alpha t} - e^{\beta t})u(t)$ after reflection at ground ($\sigma_g = 10^{-2}\ \Omega^{-1}$/m, $\epsilon_r = 1 \cdots 10$) for various values of $\beta$ at $h = 5$ m above ground; (d) induced current in transmission line corresponding to $\beta$ value (c) case 5 of Fig. 9 for comparison.

due to the superposition of the incident and ground reflected waves. The rise parameter $\beta$ has more influence on the electric field than the decay parameter $\alpha$. The induced current on the transmission line is somewhat independent of the detailed field shape because the time constant of the response is quite large compared with that of the field.

### D. The Current Return Path

The wire above ground forms a transmission line, typically with the imperfectly conducting ground medium as the return conductor. However, in the present situation, we have the terminating impedances connected to the rails rather than the ground. This strictly means the return current is shared by the rails and the soil medium. The rails are electrically, however weakly, connected to the ground medium. Therefore, the question arises as to whether we have a two-wire line with the return conductor placed at the interface of air and soil media or do we have an aerial wire above ground? The answer, of course, is frequency dependent. The exact nature of rail coupling to the ground has not been studied, and hence, the division of the return current into rail current and soil current is unknown in terms of its frequency dependence. The approximation of the aerial wire above ground, as opposed to a two-wire line with the rails as a return conductor, can only be justified over the high-frequency portions.

Finally, with reference to cases 1 and 2 contained in Fig. 7, the following observations can be made. Time interval to first zero crossing is 200 ns (measured) and 260 ns (calculated), and the peak currents are 202 A (measured) and 177 A (calculated) for case 1. For case 2, the time interval to first zero crossing is 150 ns (measured) and 160 ns (calculated), and the peak currents are $-272$ A (measured) and $-375$ A (calculated). Considering all of the approximations that had to be made in arriving at the computed results, such deviations are not difficult to understand, and perhaps improved modeling of the incident field will result in better computations.

It is noted that in all of the theoretical and experimental comparisons shown in Figs. 7 to 11, the computed results have the following approximations built in:

1) The incident field is modeled by a double exponential, and the sensitivity to its shape parameters has been studied.
2) The total horizontal field is estimated as a combination of the incident and ground-reflected waves.
3) The ground medium is characterized by $\epsilon_r = 1$ (overhead wire responses are insensitive for a range of $\epsilon_r$ values from 1 to 10) and $\sigma_g = 10^{-2}\ \Omega^{-1}$/m, leading to the best possible comparison between the theory and experiment.
4) The presence of the locomotive at the center of the transmission line is accounted for by modifying, with a constant multiplier, the uniform field observed in the incident electromagnetic wave. Such a modification leads us to understand and interpret the wave shape of the current responses in the transmission line.

5) The vertical electric field parallel to the terminating impedances are neglected in the present study.

## VI. Concluding Remarks

We have addressed the problem of investigating the current responses on a wire above ground situated near a hybrid type of NEMP simulator. The simulator facility is the MEMPS in Switzerland. Theoretical approaches are available in the literature for computing the transmission line responses. However, certain extraneous features were present during the experiment, e.g., the presence of a locomotive over a small portion of the overhead wire and the necessary rails, which affects the return path. In effect, the theoretical analysis is for a somewhat idealized situation, and the actual experiment was with engineering compromises present. The presence of the locomotive has a significant effect and can be empirically accounted for by modifying the incident fields over a portion of the wire.

It was also observed that the MEMPS facility generates a horizontal field parallel to the wire, which is fairly uniform over the entire 70-m length of the wire, in the absence of the wire and the locomotive. The wire responses have been studied with varying termination impedances. It is well known and observed here that the line resonances are seen if the terminations differ considerably (short or open circuit nominally) from the characteristic impedance of the wave propagation along the line.

A set of numerical experiments were performed as a part of sensitivity analysis to determine the effect of soil conductivity, local field strength variations, temporal shape of the incident field prior to combining with the ground reflections, etc. The agreement between the computations and experimental results are seen to be fair both in a qualitative and quantitative sense.

## References

[1] E. F. Vance, *Coupling to Shielded Cables*. New York: Wiley, 1987.
[2] A. S. Smith, *Coupling of External Electromagnetic Fields to Transmission Lines*. New York: Wiley, 1977.
[3] M. Aguet, M. Ianos, and C.-C. Lin, "Transient electromagnetic field coupling to long shielded cables," *IEEE Trans. Electromag. Compat.*, vol. EMC-22, no. 4, pp. 276–282, Nov. 1980.
[4] E. D. Sunde, *Earth Conduction Effects in Transmission Systems*. New York: Van Nostrand, 1949.
[5] S. Ramo, J. R. Whinnery, and T. Van Duzer, *Fields and Waves in Communication Electronics*. New York: Wiley, 1984, pp. 210–225, ch. 4.
[6] J. C. Giles, "A survey of simulators of EMP outside the source region: Some characteristics and limitations," in *Proc. NEM, 1984* (Baltimore, MD).
[7] H. D. Bruens, "Pulserregte elektromagnetische Vorgaenge in dreidimensionalen Stabstrukturen," Masters thesis, Univ. German Federal Armed Forces, Hamburg, West Germany, 1985.